Kinetics and crystal structure of a mutant Escherichia coli alkaline phosphatase (Asp-369 → Asn): A mechanism involving one zinc per active site

3 AUTHORS, INCLUDING:

Kinetics and crystal structure of a mutant *Escherichia coli* alkaline phosphatase (Asp-369 → Asn): A mechanism involving one zinc per active site

THOMAS T. TIBBITTS, XU XU,[1] AND EVAN R. KANTROWITZ

Department of Chemistry, Merkert Chemistry Center, Boston College, Chestnut Hill, Massachusetts 02167-3860

Abstract

Using site-directed mutagenesis, an aspartate side chain involved in binding metal ions in the active site of *Escherichia coli* alkaline phosphatase (Asp-369) was replaced, alternately, by asparagine (D369N) and by alanine (D369A). The purified mutant enzymes showed reduced turnover rates (k_{cat}) and increased Michaelis constants (K_m). The k_{cat} for the D369A enzyme was 5,000-fold lower than the value for the wild-type enzyme. The D369N enzyme required Zn^{2+} in millimolar concentrations to become fully active; even under these conditions the k_{cat} measured for hydrolysis of *p*-nitrophenol phosphate was 2 orders of magnitude lower than for the wild-type enzyme. Thus the k_{cat}/K_m ratios showed that catalysis is 50 times less efficient when the carboxylate side chain of Asp-369 is replaced by the corresponding amide; and activity is reduced to near nonenzymic levels when the carboxylate is replaced by a methyl group. The crystal structure of D369N, solved to 2.5 Å resolution with an *R*-factor of 0.189, showed vacancies at 2 of the 3 metal binding sites. On the basis of the kinetic results and the refined X-ray coordinates, a reaction mechanism is proposed for phosphate ester hydrolysis by the D369N enzyme involving only 1 metal with the possible assistance of a histidine side chain.

Alkaline phosphatase (EC 3.1.3.1) is a phosphomonoesterase exhibiting a high degree of sequence homology among species from bacteria to man. In *Escherichia coli* it functions as a scavenger for phosphate from a wide variety of substrates, where it is active in the periplasmic space as a homodimer containing 4 zinc and 2 magnesium ions (Anderson et al., 1975, 1976; Coleman et al., 1983). Dependence of catalysis on metal binding was first demonstrated by kinetic reactivation of the apo-enzyme by addition of zinc (Anderson et al., 1975), and later by ^{31}P and ^{113}Cd NMR spectroscopy (Hull et al., 1976; Gettins & Coleman, 1983a, 1983b, 1984b; Gettins et al., 1985). Hydrolysis proceeds through a phosphoseryl intermediate with subsequent release of an alcohol and inorganic phosphate (Schwartz & Lipmann, 1961). In the presence of a phosphate acceptor such as ethanolamine or Tris, the enzyme also catalyzes a transphosphorylation reaction (Dayan & Wilson, 1964; Wilson et al., 1964).

The X-ray structure of the wild-type *E. coli* enzyme, first solved to 2.8 Å resolution (Sowadski et al., 1981, 1983, 1985) has been further refined to a resolution of 2.0 Å with an *R*-factor of 0.22 (Kim & Wyckoff, 1989, 1991). Crystals form in the presence of Zn^{2+}, Mg^{2+}, and phosphate with I222 space group symmetry. The molecular dyad axis, relating the 2 449-residue subunits (A, B), is noncrystallographic. The 2 active sites, one on each monomer, are about 30 Å apart. In each active site there are 3 metal binding sites (M1, M2, M3); 2 sites are occupied by zinc (M1 and M2) and the third site contains magnesium (M3). These are located in a small pocket close to Ser-102, which is transiently phosphorylated during the reaction. Zinc at the M1 site is pentacoordinated; the ligands are the imidazole nitrogens of His-331 and His-412, both carboxylate oxygens of Asp-327

---

in a bidentate fashion and the phosphate oxygen designated as O1. At the M2 site, zinc is coordinated tetrahedrally — by O2 of the phosphate, the imidazole nitrogen of His-370, and the carboxylate oxygens of Asp-51 and Asp-369. Magnesium, bound at the M3 site, forms an octahedral arrangement with 6 ligands: 3 water molecules, the carboxylate oxygens of Asp-51 and Glu-322, and the hydroxyl oxygen of Thr-155. The side-chain carboxylate of Asp-51 is thus doubly coordinated, forming a bridge between the M2 and M3 sites. Inorganic phosphate is bound in a similar fashion, bridging zinc atoms in the M1 and M2 sites (Kim & Wyckoff, 1989, 1991). Phospholipase C from *Bacillius cereus* (Hough et al., 1989) and P1 nuclease from *Penicillium citrinum* (Volbeda et al., 1991) are phosphoesterases that also have metal triads at their active site, with an arrangement of side-chain ligands similar in many respects to alkaline phosphatase.

A mechanism for 2-metal ion catalysis in alkaline phosphatase has been proposed based on NMR spectroscopy (Gettins & Coleman, 1984a, 1984b; Coleman, 1987) and structural models of the Zn^{2+}- and Cd^{2+}-bound enzymes provided by X-ray crystallography (Kim & Wyckoff, 1989, 1991). In the initial step of the reaction, the metal cation bound at the M2 site in the enzyme–substrate complex activates the hydroxyl of Ser-102 for nucleophilic attack at the phosphorous, whereas the metal bound at the M1 site assists the substrate-derived alcohol to leave. The metal at the M1 site then activates a water molecule for nucleophilic attack of the phosphoseryl-enzyme intermediate, thus giving a double-displacement mechanism with retention of configuration at the phosphorus (Jones et al., 1978).

Site-specific mutagenesis has been used to probe the catalytic mechanism of alkaline phosphatase by substituting different amino acid side chains to replace residues involved in binding metals and substrates at the active site (Xu & Kantrowitz, 1992, 1993; Janeway et al., 1993). Recently, kinetic studies of the mutated proteins have been combined with X-ray crystallography and molecular dynamics calculations to help visualize structure–function relationships in alkaline phosphatase and to improve the understanding of the general features of catalysis in metal-containing enzymes (Murphy et al., 1993; Murphy & Kantrowitz, 1994).

In this study, site-specific mutagenesis was used to substitute alanine and asparagine for Asp-369, 1 of 2 aspartate residues whose carboxylate side chain serves as a ligand for metal cat-

ions at the M2 binding site (Fig. 1; Kinemage 2). The purified D369A, D369N and wild-type enzymes were assayed to determine experimental conditions for optimal activity, and to compare, in each case, the effects of Zn^{2+} concentration and the presence of a phosphate acceptor on catalysis. The D369N enzyme was crystallized for X-ray structural analysis to determine the precise orientation of side chains and the positions of metal ions near the active site. The effects of the amino acid replacements on catalysis were therefore assessed using both kinetic results and structural information provided by detailed comparison of the atomic coordinates for the D369N and wild-type enzymes (see Kinemage 1). Based on our findings, we propose a new catalytic mechanism for phosphate ester hydrolysis by the D369N enzyme.

Results

Steady-state kinetic parameters of the D369N and D369A enzymes

The k_{cat} values for the D369N and D369A enzymes at pH 8.0, determined both in the presence and absence of a phosphate acceptor, are significantly lower than that of the wild-type enzyme. In the absence of a phosphate acceptor (0.1 M MOPS) where the hydrolysis activity of the enzyme is measured, the k_{cat} value of the D369N enzyme is $0.4 \, s^{-1}$, about 100-fold less than that of the wild-type enzyme (see Table 1A). Under the same conditions, the k_{cat} of the D369A enzyme is significantly lower than that observed for the D369N enzyme, and approximately 5,000-fold lower than that of the wild-type enzyme. The mutant enzymes also show a 2–300-fold increase in K_m compared with the wild-type enzyme; overall then 200- to 10^6-fold decreases are exhibited in the k_{cat}/K_m ratio.

Steady-state kinetic parameters for the wild-type, the D369N, and the D369A enzymes were also examined in 1.0 M Tris buffer at pH 8.0. Because Tris can act as a phosphate acceptor, the rate
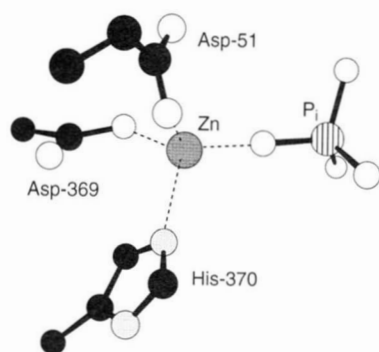

Fig. 1. The M2 metal binding site based on the crystal structure of wild-type alkaline phosphatase. The phosphate is also a ligand to zinc bound at the M1 site, and the Asp-51 carboxylate serves as a ligand for magnesium at the M3 site.

Table 1. *Kinetic parameters of the wild-type and mutant enzymes at pH 8.0*[a]

Enzyme[b]	k_{cat}[c] (s^{-1})	K_m (μM)	k_{cat}/K_m $(M^{-1} \cdot s^{-1})$	Buffer
A. In the absence of a phosphate acceptor				
Wild type	44.5	9.4	4.7×10^6	0.1 M MOPS, pH 8.0[d]
D369N	0.4	17.6	2.2×10^4	0.1 M MOPS, pH 8.0
D369A	0.01	2,941	3.4	0.1 M MOPS, pH 8.0
B. In the presence of a phosphate acceptor				
Wild type	80.5	21.1	3.8×10^6	1.0 M Tris, pH 8.0
D369N	2.3	59.7	3.8×10^4	1.0 M Tris, pH 8.0
D369A	—[e]	—	—	1.0 M Tris, pH 8.0

[a] Assays were performed at 25 °C in the buffer indicated using *p*-nitrophenyl phosphate as substrate.

[b] The enzymes were stored in TMZP buffer.

[c] The k_{cat} values are calculated from the V_{max} using a dimer molecular weight of 94,000. The k_{cat} per active site would be half the value indicated.

[d] For the MOPS buffer, the ionic strength was adjusted to 0.585 with NaCl.

[e] No activity above the background was detectable.

observed is the sum of the transphosphorylation and the hydrolysis reactions (Wilson et al., 1964; Trentham & Gutfreund, 1968; Gettins et al., 1985). Under these conditions, the D369N enzyme exhibited a 40-fold reduction in k_{cat} compared to the wild-type enzyme (Table 1B), whereas the D369A enzyme showed no detectable activity. A 3-fold increase in the K_m was also observed for the D369N enzyme, therefore the k_{cat}/K_m ratio for the D369N enzyme decreased 100-fold compared with that for the wild-type enzyme.

Influence of zinc on the kinetic parameters of the wild-type and mutant enzymes at pH 8.0

Because Asp-369 is a ligand at the M2 site, mutation of this residue might be expected to reduce the zinc affinity of the enzyme. Therefore, the effect of zinc on the activity of the mutant enzymes was examined. The mutant enzymes were first dialyzed against 0.01 M Tris, 1 mM Mg^{2+}, pH 7.4, buffer in order to reduce the free zinc concentration. Initially, 0.4 mM of Zn^{2+} was added, and the activity of the enzyme was determined in 0.01 M Tris, 0.4 mM Zn^{2+} buffer, pH 8.0, at various time intervals. A time-dependent zinc activation was observed with a half-time of 10 min (Fig. 2A). No analogous zinc activation is observed for the wild-type (Fig. 2B) or the D369A enzymes (data not shown). Zinc activation was also determined after preincubating the enzyme (0.1 μM) for 1–2 h with increasing concentrations of zinc in 0.01 M Tris buffer, pH 7.4. The hydrolysis activity was then determined in 0.01 M Tris, pH 8.0, buffer with the same concentration of Zn^{2+} as contained in the preincubation buffer (Fig. 3). The fully activated D369N enzyme exhibited about 50-fold higher activity than the enzyme that was not treated with
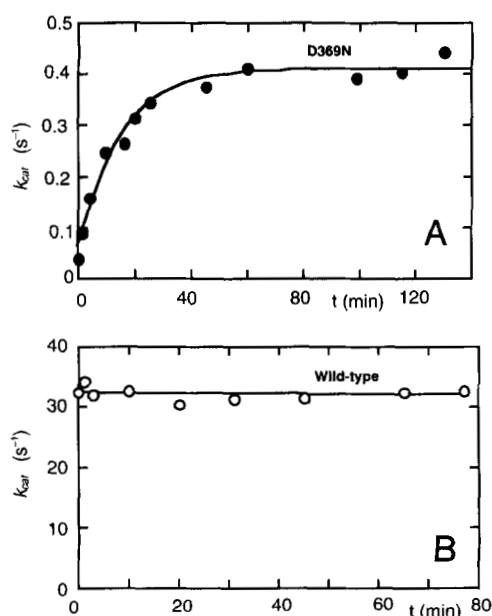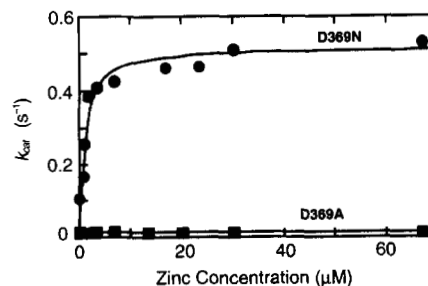

Fig. 3. The effect of pretreating with different Zn^{2+} concentrations on the activity of the D369N and D369A enzymes. The enzymes were incubated at room temperature for 1–2 h in the presence of increasing concentrations of Zn^{2+} in 0.01 M Tris, pH 7.4. Activities were then determined at pH 8.0 in 0.01 M Tris buffer with the same Zn^{2+} concentrations. All reactions were performed at 25 °C with *p*-nitrophenyl phosphate as substrate.

zinc, and the fully zinc-activated D369N enzyme had about 1% of the activity of the wild-type enzyme (Fig. 2). The apparent zinc dissociation constant calculated from these data for the D369N enzyme is about 10^{-6} M compared to 10^{-8} M for the wild-type enzyme (Coleman et al., 1983).

Refinement of the D369N enzyme X-ray structure

The D369N enzyme was crystallized under conditions similar to those previously used for the wild-type, D101S, and D153H enzymes (Kim & Wyckoff, 1991; Chen et al., 1992; Murphy et al., 1993). The space group of the crystals of the D369N enzyme, I222, was the same as the wild-type enzyme, and the unit cell dimensions ($a = 194.4$ Å, $b = 167.3$ Å, $c = 76.3$ Å) differed from those of the wild-type by less than 0.5%. Therefore, the coordinates of the wild-type enzyme (Kim & Wyckoff, 1991) were used as an initial model for the structural refinement of the D369N enzyme.

The refinement was begun without any water molecules included in the model. These were gradually added as they were identified in $2F_o - F_c$ and $F_o - F_c$ difference maps, first as single molecules and later in symmetric pairs. The final positions of 105 symmetry-related pairs of water molecules and 84 nonsymmetric placed waters identified in the D369N enzyme were tested for surface accessibility using the surface probe algorithm (Lee & Richards, 1971) implemented in QUANTA (Molecular Simulations). Approximately 50% of the symmetric and 10% of the nonsymmetric water molecules in the homodimer are internal with no area exposed to bulk solvent (see Kinemage 3).

The final refined coordinates for the D369N enzyme were analyzed using PROCHECK (Laskowski et al., 1993), which indicated, using several stereochemical criteria, that the overall quality of the refined model was comparable to other structures determined at 2.5 Å resolution. The Ramachandran plot of dihedral angles is shown in Figure 4. The uncertainty in the refined coordinates for D369N was estimated at 0.30–0.45 Å, from a Luzatti plot showing the resolution dependence of the R-factor (Fig. 5). The overall R-factor, calculated to 2.5 Å resolution, was 0.189. Furthermore, RMS deviations from ideal bond lengths, ideal bond angles, and ideal atom contacts were calculated using XPLOR (Brünger, 1992), and shown in Table 2.

Fig. 2. The effect of zinc on the D369N (**A**) and wild-type enzymes (**B**). The enzymes were dialyzed extensively against 0.01 M Tris, 1 mM Mg^{2+}, pH 7.4, buffer before use. At time 0, 0.4 mM Zn^{2+} was added to the enzyme and the activity was determined in 0.01 M Tris, pH 8.0, buffer with 0.4 mM Zn^{2+}. Reactions were performed at 25 °C with *p*-nitrophenyl phosphate as substrate.
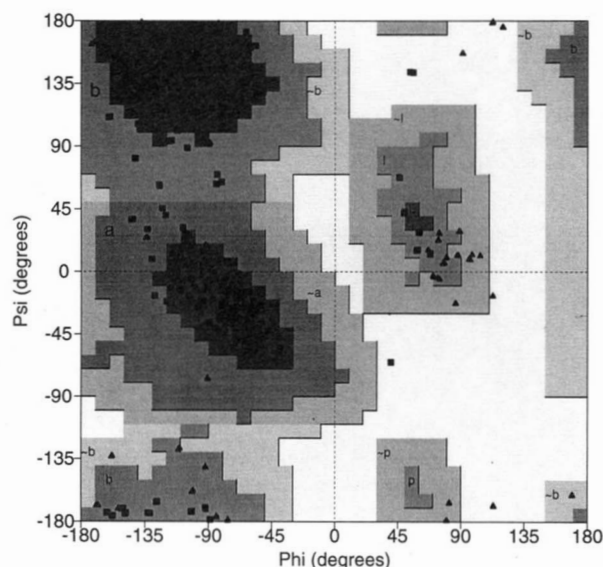
Fig. 4. Ramachandran plot showing that 92% of the residues are in the most favored regions (A, B, L), 7.5% in the additional allowed regions (a, b, l, p), and only 0.5% (2 residues on each chain) in the disallowed regions (lightest areas). Glycine and proline residues are shown as triangles.

Table 2. *Geometric and energetic analysis of the refined model for the D369N enzyme: RMS deviations from ideal values*

	RMSD
Bonds (V)	0.00785
Angles (deg)	2.49
Dihedral (deg)	23.8
Improper (deg)	1.03

E322D enzyme (T. Tibbitts, X. Xu, & E.R. Kantrowitz, unpubl.). The anion is stabilized by a hydrogen bond with the indole nitrogen of Trp-268 and electrostatic attraction to 2 guanidino groups located on the side chains of Arg-267 and Arg-292.

The active site in the D369N enzyme

As the refinement progressed, it became apparent from the electron density maps that the D369N enzyme differed significantly from the wild-type enzyme at the active site (see Kinemage 2). The refined positions of side chains at the D369N active site are shown in Figure 7 with the corresponding electron density. The density maps showed that phosphate, normally held by 2 Zn^{2+} atoms in the wild-type active site, was coordinated by a single metal atom in the mutant. This single metal was bound to the protein close to the position of the M1 site in the wild-type enzyme. Lack of sufficient density at the M2 and M3 sites indicated that these sites are unoccupied at millimolar concentrations of Zn^{2+} and Mg^{2+}.

Amino acid side chains, which normally bind metals to the M2 and M3 sites in the wild-type enzyme, were reoriented in the D369N enzyme, indicating a different pattern of hydrogen bonding (Table 3). Note that the lowest-energy orientation of the asparagine side chain at position 369 has the carbonyl oxygen hydrogen bonded to the main chain and the amide nitrogen pointing toward the unoccupied M2 site. One hydrogen of the amide is bonded to a water molecule, whereas the other is bonded to a side chain carboxyl of Asp-51 and weakly bonded to the imidazole nitrogen acceptor of His-370. Interestingly, the imidazole nitrogen acceptor of His-370 and the hydroxyl oxygen donor of Ser-102 are also close enough in the mutant structure to form a weak hydrogen bond.

Stereo pairs of the refined atomic coordinates, portraying the fit of the model to the electron density map, are shown for 2 domains in the D369N enzyme (Figs. 6, 7). These domains were chosen to include (1) side chains belonging to residues at the secondary anion binding site, first identified in this D369N alkaline phosphatase structure, and (2) active site residues that normally bind a metal or phosphate ligand.

A secondary anion binding site in the D369N enzyme

A second binding site for anions, which may be occupied by either phosphate or sulfate, was found in the D369N enzyme (Fig. 6), and recently also found in electron density maps of the
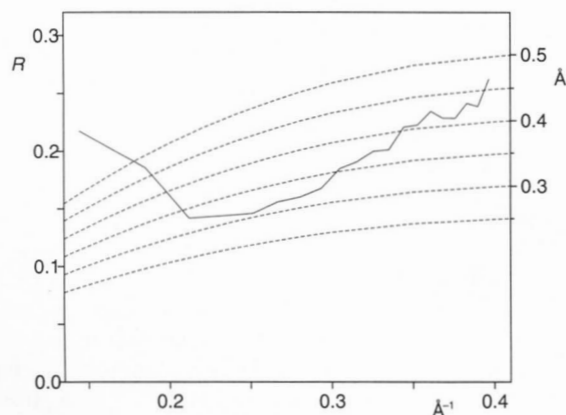
Comparing the crystal structures of the D369N and wild-type enzymes

The D369N enzyme was compared to the wild-type enzyme over the entire structure and separately in each metal binding site (Table 4; Kinemages 1, 2). This was done by calculating the RMS displacement (RMSD) for the C_α and side-chain atoms. The largest differences in C_α positions were for residues near Glu-408 having relatively weak density in the maps—indicating a flexible or disordered loop region. The temperature factors of the side chains in each metal site are also presented in Table 4. Side chains liberated by the vacancies at the M2 and M3 metal binding sites (e.g., D51, H370, T155) generally showed larger

Fig. 5. Luzatti plot showing the final *R*-factors, by resolution shell, for the D369N crystal structure. The expected uncertainty in the refined X-ray coordinates of the D369N mutant alkaline phosphates is 0.30–0.45 Å, as indicated by the set of dashed lines (Luzatti, 1952; Brünger, 1992).
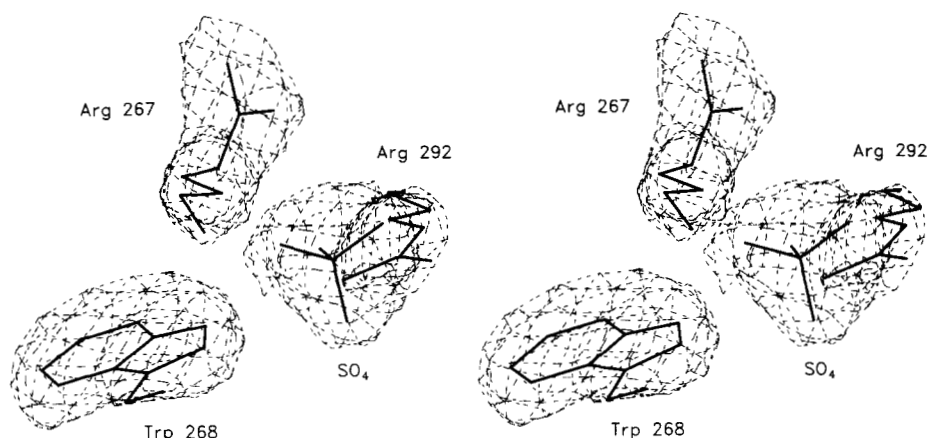
Fig. 6. Stereo pair showing the electron density of the second anion binding site found in D369N alkaline phosphatase. The ligand at this site, which may be either phosphate or sulfate, was modeled as sulfate during the refinement. Figures 6, 7, and 8 were produced using the program SETOR (Evans, 1993).

increases in temperature factor than nearby side chains, which do not interact directly with the metals.

The positions of the side chains and metals at the active sites of the D369N and wild-type enzymes are shown superposed in Figure 8 and Kinemage 2). At the M1 site, the histidine imidazole rings have rotated slightly, but zinc is still bound close to the same position in the 2 enzymes. Ser-102 moved slightly into the M2 site, 0.2 Å closer to His-370. The vacancies at M2 and M3, expected to leave free carboxylate anions at Asp-51 and Glu-322, apparently destabilized formation of the salt bridge between Lys-328 and Asp-153. In the D369N enzyme, Lys-328 showed a significant shift from the wild-type position, accompanied by increase in temperature factor, as did most of the side chains in the helical region containing Glu-322 to Lys-328. Furthermore, there is density indicating a K328–D51 salt bridge, which positions the positively charged ϵ-amino of Lys-328 closer to the vacant M3 binding site in the D369N enzyme.

Discussion

The Asp → Asn replacement affects all 3 metal sites

Aspartate at position 369 is necessary for coordinating metals at the M2 site. Its replacement by asparagine both disrupts metal

binding and dictates a different network of hydrogen bonding interactions, which influences the relative positions of all the other side chains around the M2 site. The absence of the metal cation at M2, combined with the different side-chain positions around the M2 site, in turn affects the binding of phosphate to the enzyme, the orientation of the side-chain ligands around M1, and hence the affinity for Zn^{2+} at the M1 site. Similarly, at the M3 site both positions of the side chains and binding affinity for Mg^{2+} are affected. The substantially different arrangement of side chains in the active site of the D369N enzyme, described below, provides an explanation for the observed kinetic results, and suggests a catalytic reaction mechanism for the mutant enzyme differing from the wild-type enzyme.

At the M2 site, the amide nitrogen of the asparagine side chain substituted at 369 is a poor ligand for metal cations, compared to the carboxylate oxygen it replaced. Because the crystal stabilization buffer for wild-type and D369N enzymes contained 10 mM $ZnCl_2$, the vacancy at the M2 site indicates that the dissociation constant for Zn^{2+} at this site was increased by several orders of magnitude, to at least 10^{-2} M under these conditions. Consequently, vacancy at the M2 metal site permits the phosphate oxygen, Asp-51 carboxylate, and His-370 imidazole ligands to reorient in order to form stabilizing interactions with nearby chemical groups.
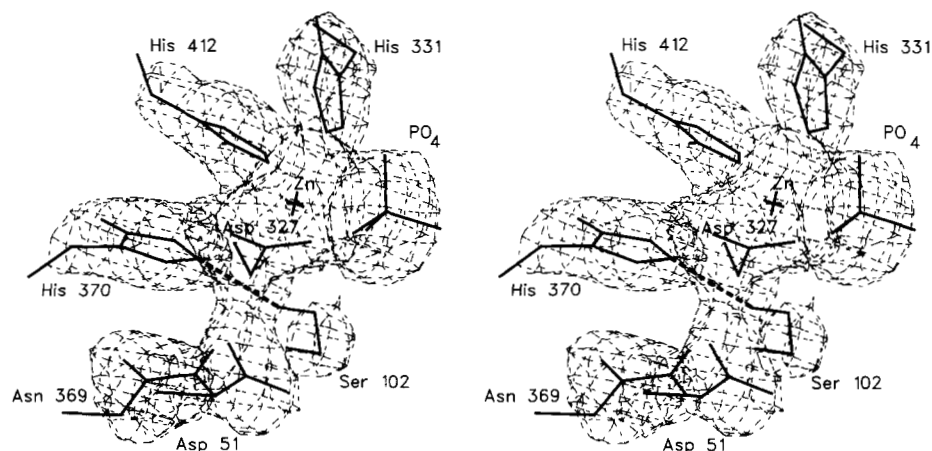

Fig. 7. Stereo pair showing electron density at the active site in D369N alkaline phosphatase. This map is an $F_o - F_c$ electron density map, calculated with the Zn^{2+}, phosphate, and the side chains of active site residues omitted. The positions of metal atoms that normally occupy the M2 and M3 metal coordination sites in the wild-type enzyme are in the regions outside the chosen contour ($\sigma = 2.7$). Freed from its normal role as a coordinating ligand to Zn at the M2 site, the imidazole nitrogen of His-370 has formed a hydrogen bond with the γ-hydroxyl of Ser-102 in the D369N mutant. We propose that His-370 helps to abstract the proton from the seryl oxygen, thus activating it for nucleophilic attack at the phosphate group on the bound substrate.

Table 3. *Hydrogen bonds in D369N near the substitution site*[a]

Donor	Atoms 1-2	Atoms 3-4	Accept	$\angle 123°$	D_{23} (Å)
G52	N···H	OD1-CG	N369	153	2.0
S102	N···H	O2-P	PO$_4$	169	2.2
	OG···HG	NE2-CD2	H370	147	2.7
S147	OG···HG	OE1-CD	E322	94	2.5
T155	OG1···HG1	OH2	H$_2$O	164	1.9
	OG1···HG1	OE2-CD	E322	110	2.5
R166	NH1···HH12	O2-P	PO$_4$	114	2.4
D327	N···H	O-C	D51	113	2.3
	N···H	O-C	A324	119	2.8
K328	N···H	O-C	A324	168	2.8
	NZ···HZ1	O-C	A324	155	2.5
	NZ···HZ2	OD2-CG	D51	111	2.9
H331	N···H	O-C	D327	151	2.0
	N···H	O-C	K328	118	2.6
	ND1···HD1	O-C	Q410	122	2.2
N369	ND2···HD21	OH2	H$_2$O	154	1.9
	ND2···HD22	OD1-CG	D51	132	2.0
	ND2···HD22	NE2-CD2	H370	110	2.9
H370	N···H	OD1-CG	N369	128	2.2
	ND1···HD1	O-C	A371	124	2.9
H412	ND1···HD1	O-C	T100	139	2.2

[a] Angles between the atoms ($\angle$ 123°) and distances (D_{23}) listed are for the B chain. Atoms are identified by their names in the Brookhaven PDB file.

Phosphate binds to the D369N enzyme about 2 Å away from its location in the wild-type enzyme and is more exposed to the surface. In the wild-type enzyme, phosphate is coordinated by 2 zinc atoms and is further stabilized by the guanidinium group

Table 4. *Comparison of the coordinates for the D369N and wild-type enzymes*

Residues included	RMSD (Å)		Side chain B (Å^2)	
	C$_\alpha$	Side chain	D369N	WT
All	0.28	0.88	22	18
M1 site	0.21	0.87	33	12
M2 site	0.25	0.72	19	7.3
M3 site	0.30	0.79	20	9.5
D153/K328	0.26	1.1	39	11
Active site	0.24	0.95	31	9.5

of Arg-166 through 2 hydrogen bonding interactions. In the D369N enzyme, the side chain of Arg-166 is not well defined by the density, and its position in the refined model indicates that it forms only 1 hydrogen bond to the phosphate. The temperature factor (B factor) of the phosphate group in the D369N structure is 49.7 Å^2, which is significantly higher than that reported for the wild-type enzyme, 20.1 Å^2 (Kim & Wyckoff, 1991). These results are consistent with our observation that the binding affinity of the D369N enzyme for phosphate is lower than that shown by the wild-type enzyme.

At the M1 site, substitution at position 369 also caused zinc to bind less tightly. This behavior may be caused, in part, by the weakened affinity for phosphate, which can no longer act as a stabilizing bridge between the M1 and M2 sites. The dissociation constant for zinc at the M1 site increased from 10^{-8} to 10^{-6} M, and full activation of D369N enzyme occurred only at micromolar concentrations of the metal. These data indicate that zinc can be removed from the D369N enzyme during dialysis, unlike the wild-type enzyme. When full occupancy of M1 is achieved at micromolar concentrations of zinc, the D369N enzyme is fully activated.

The single mutation of Asp-369 also resulted in destabilization of metal binding at the third site, M3, in the D369N enzyme.
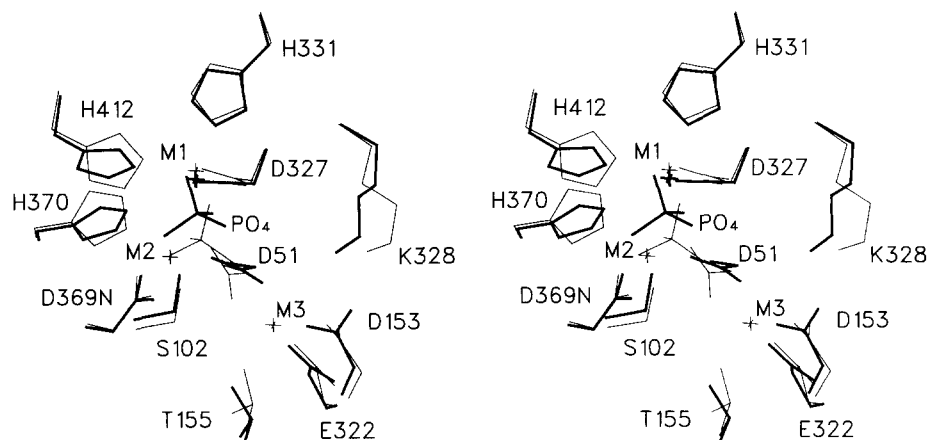

Fig. 8. Stereo pair comparing the positions of side chains, metals, and phosphate in the active sites of the D369N enzyme (thick lines) and the wild-type enzyme (thin lines). At the M1 site, zinc is bound close to the same location in both enzymes (crosses), but phosphate (PO$_4$) is more exposed to the surface in the D369N structure. At the M2 site, zinc is bound in the wild-type (cross) but not the mutant enzyme. This permits S102 to move slightly closer to H370 and the asparagine introduced at position 369 (D369N). The M3 site normally contains Mg^{2+} (cross) with 3 water molecules (not shown) in the wild-type enzyme; in the mutant enzyme this space is partially filled by 1 water molecule (not shown), the carboxylate side chain of D51, and the ε-amino group of K328. The 2 sets of atomic coordinates were aligned using Quanta to minimize the RMSD of the Cα atoms before making this comparison.

The low electron density in $2F_o - F_c$ maps showed that M3 is vacant and thus the dissociation constants for both Mg^{2+} and Zn^{2+} at the M3 site must be at least 10^{-2} M in the crystal-stabilizing buffer. Side chains around the M3 site, serving as ligands to magnesium in the wild-type enzyme, have also shifted their positions. The 2 carboxylate oxygens of Glu-322 (OE1 and OE2) now form hydrogen bonds to 2 hydroxyl groups, 1 on either side. The hydrogen bond between OE1 and the side chains of Ser-147, present in the wild-type, is retained. However, the OE2 oxygen of Glu-322 and the side chain hydroxyl oxygen of Thr-155, both of which served as ligands in the wild-type enzyme, form a new hydrogen bond between them in the D369N enzyme. Finally, Asp-51 serves a special role in the wild-type enzyme, acting as a carboxylate ligand that bridges the M2 and M3 sites. In the D369N mutant, the side chain of Asp-51 has a different orientation, interacting with the side-chain amino group of Lys-328. This result may indicate that binding of a metal ion at the M2 site is prerequisite for correct placement of Asp-51 toward coordination of a metal ion at the M3 site.

The D369N enzyme catalyzes the reaction by a different mechanism

The D369N enzyme cannot catalyze the hydrolysis of phosphate esters by the same mechanism as the wild-type enzyme because of the absence of the metal ion in the M2 site. In the active site of the mutant, the His-370 side chain has moved to within 2–3 Å of the hydroxyl oxygen of Ser-102. This hydroxyl, which is phosphorylated and dephosphorylated during the reaction, is hydro-

gen bonded to the imidazole nitrogen of His-370 in the mutant structure. This would suggest a role for His-370: to weaken the serine O–H bond and therefore strengthen the nucleophilic character of the serine hydroxyl oxygen sufficiently to attack the phosphorous. In this scheme (Fig. 9) the D369N enzyme (E) can bind the substrate (ROP) to form the enzyme–substrate complex (**E·ROP**). The phosphate of the substrate is held loosely in the active site by zinc and Arg-166. In the **E·ROP** complex, His-370 stabilizes the partially deprotonated form of Ser-102 necessary for nucleophilic attack at the phosphorus atom. The hydroxyl oxygen of Ser-102 attacks the phosphate apically as the zinc in the M1 site stabilizes the developing negative charge on the leaving RO^-. In the covalent phosphoenzyme intermediate (**E–P**) a hydroxyl nucleophile is available for apical attack on the phosphorus, to displace Ser-102, with His-370 again stabilizing the developing negative charge.

Given the large changes in the active site and the loss of 2 metal ions, it is also possible that a single-displacement mechanism, involving a zinc-activated water or Tris hydroxyl, is operational in the D369N enzyme. The proposed double-displacement mechanism, however, offers an explanation for the relative activities of the D369A, D369N, and wild-type enzymes, by considering the environment of the seryl oxygen nucleophiles in each case. The X-ray structure of the D369N enzyme indicates that the side-chain carbonyl of Asn-369 forms hydrogen bonds with main-chain nitrogen donors at Gly-52 and His-370. Furthermore, the side-chain nitrogen of Asn-369 forms hydrogen bonds with the imidazole nitrogen of His-370 and carboxylate side chain of Asp-51. Because none of these H bonds are possible
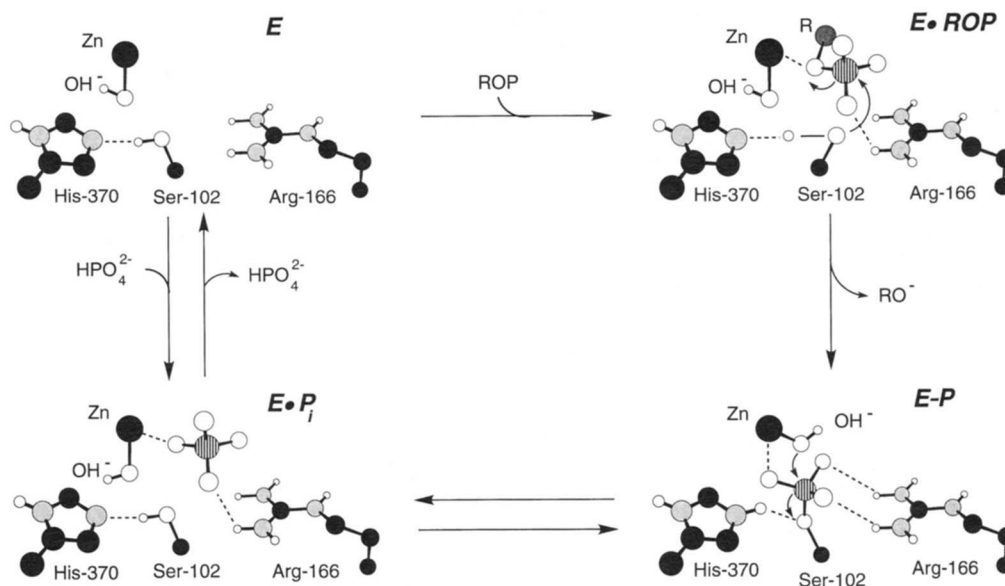

Fig. 9. A proposal for the mechanism of the D369N enzyme based on the X-ray structure with phosphate bound. The enzyme, after purification, exists as a mixture of free enzyme (**E**, top left) and the enzyme complexed with inorganic phosphate (**E·P$_i$**, bottom left). The free enzyme can bind the substrate (ROP) to form a Michaelis complex (**E·ROP**, top right). The phosphate of the substrate is held loosely in the active site by zinc and Arg-166. In the **E·ROP** complex, the seryl O–H bond is sufficiently weak to increase the nucleophilic character of the serine hydroxyl oxygen. The hydroxyl of Ser-102 attacks the phosphate apically as the zinc stabilizes the developing negative charge on the leaving group RO^-. In the covalent phosphoenzyme intermediate (**E–P**, bottom right) a hydroxyl nucleophile is available for apical attack on the phosphorus, to displace Ser-102, with His-370 stabilizing the developing negative charge. Hydroxyl ligands shown bound to the Zn^{2+} atoms are in equilibrium with water; their positions are based on Mn^{2+}-ESR and NMR dispersion studies of the M1 site in the wild-type enzyme (Schultz et al., 1989).

in the D369A enzyme, we conclude that these interactions may facilitate catalysis in the D369N enzyme by restraining the position of the His-370 side chain near the catalytic serine. Still, in the D369N enzyme His-370 only partially fulfills the major role proposed for zinc at the wild-type M2 site, which is to stabilize the formation of a serine oxyanion that can attack the phosphate. Thus in the respective **E·ROP** complexes, the character of the Ser-102 side chain differs markedly: in the D369A enzyme it is the weakly nucleophilic O–H, in the D369N enzyme it is partially activated O–H, and in the wild-type enzyme it is the fully activated and strongly nucleophilic O⁻. Other structural differences may be important as well. For example, His-370 cannot fulfill the second role played by zinc at the M2 site, which is to place the phosphate target in optimum position for nucleophilic attack.

The X-ray structure of the D369N enzyme leads us to propose yet a third role for zinc bound at the M2 site. Apparently it influences the metal occupancy at the M3 site, by positioning the carboxylate bridge (Asp-51) needed to bind metals at the M3 site. Phospholipase C and P1 nuclease include an aspartate side chain, analogous to Asp-51, which serves as a bridge between 2 of the 3 metal sites. Aspartate bridges may thus be a common feature in enzymes containing multiple metal sites. Our results suggest that 1 role of these Asp bridges may serve to link the occupancy of the 2 bridged sites, perhaps to promote a specific sequence of metal binding.

Combined use of site-specific amino acid substitution, kinetic characterization, and X-ray crystallography has demonstrated the importance of Asp-369 to metal binding at the M2 site and yielded additional information about the function of the zinc cation normally bound at the M2 site. Moreover, this study produced a novel phosphoesterase (D369N) that contains only a single zinc atom at the active site. The mechanism proposed for this enzyme—which has histidine and a single metal ion assisting in phosphate ester hydrolysis—is consistent with the low, but significant catalytic activity of the D369N enzyme and explains the very low activity of the D369A enzyme. Further study of mutated forms of *E. coli* alkaline phosphatase as model systems should eventually lead to a fundamental understanding of catalysis in enzymes that contain multiple zinc and/or magnesium metals at their active sites.

Kinemages

Three kinemages are included to demonstrate the similarity of the wild-type and D369N protein backbones, to highlight the differences at the active site, and to indicate solvent positions in D369N. These computer files permit interactive switching and overlay comparisons of the wild-type and D369N X-ray structures.

Materials and methods

Chemicals

Agar, ampicillin, glycerol, MOPS, *p*-nitrophenyl phosphate, and sodium dihydrogen phosphate were purchased from Sigma Chemical Co. Tris, electrophoresis-grade agarose, enzyme-grade ammonium sulfate, and sucrose were purchased from ICN Biomedicals. Tryptone and yeast extract were obtained from Difco Laboratories. Analytical-grade $MgCl_2$ and $ZnSO_4$ were from

Mallinckrodt and Fisher Scientific. DNA sequencing reagents were purchased from U.S. Biochemicals. Restriction endonucleases, T4 DNA ligase, the Klenow fragment of DNA polymerase I, and T4 polynucleotide kinase were obtained from both U.S. Biochemicals and New England Biolabs and used according to the suppliers' recommendations. DNA fragments were isolated from agarose gels using glass beads employing the US Bioclean kit from Bio 101. The oligonucleotides required for site-specific mutagenesis were synthesized by Operon Technologies Inc.

Strains

The *E. coli* K12 strain MV1190 (Δ(*lac-proAB*), *supE*, *thi*, Δ(*sri-recA*) 306::Tn10(tetʳ)/F′ *traD36*, *proAB*, *lacI�q*, *lacZ*ΔM15), and the M13 phage M13K07 were obtained from J. Messing. The Δ*phoA E. coli* K12 strain SM547 (Δ(*phoA-proC*), *phoR*, tsx::Tn5, Δ*lac*, *galK*, *galU*, *leu*, strʳ) was a gift from H. Inouye. The strain CJ236 (*dut-1*, *ung-1*, *thi-1*, *relA-1*/pCJ105 (Cmʳ)) was a gift from T. Kunkel.

Construction of the D369N and D369A enzymes by site-specific mutagenesis

The mutational changes at position 369 of alkaline phosphatase were introduced by the method of Kunkel (Kunkel, 1985; Kunkel et al., 1987) as modified by Xu and Kantrowitz (1991). Selection of the mutations was performed directly by sequencing, and the DNA fragment containing the mutation site was then recloned and confirmed by procedures described previously (Chaidaroglou et al., 1988; Xu & Kantrowitz, 1991). In this fashion, the plasmids pEK208 and pEK209, which carry the D369A and D369N mutations, respectively, were constructed.

Expression of the wild-type and the mutant alkaline phosphatases

E. coli SM547 was used as the host strain for expression of both the wild-type and mutant alkaline phosphatases. This strain contains a chromosomal deletion of the *phoA* gene and a mutation in the *phoR* regulatory gene.

Purification of the wild-type and mutant alkaline phosphatases

The wild-type, D369A, and D369N enzymes were isolated from the plasmid/strain combinations pEK48/SM547, pEK208/SM547, and pEK209/SM547, respectively, by methods previously described (Chaidaroglou et al., 1988). Enzyme purity was judged by SDS-polyacrylamide gel electrophoresis (Laemmli, 1970).

Determination of protein concentration

The concentration of the wild-type enzyme was determined by absorbance measurements at 278 nm with an extinction coefficient of 0.71 cm²/mg (Plocke & Vallee, 1962). The concentration of the mutant enzymes was determined by the Bio-Rad version of Bradford's dye binding assay (Bradford, 1976) using wild-type alkaline phosphatase as the standard.

Determination of enzymatic activity

Alkaline phosphatase activity was measured spectrophotometrically utilizing *p*-nitrophenyl phosphate as the substrate (Garen & Leventhal, 1960). The release of the *p*-nitrophenolate chromophore was monitored at 410 nm. The extinction coefficient of *p*-nitrophenolate was determined at each pH value used by measuring the absorbance after complete enzymatic hydrolysis of the substrate. The buffer systems used were 1.0 M Tris, 0.01 M Tris, or 0.1 M MOPS buffer at pH 8.0. The ionic strength was held constant at 0.585 with NaCl.

Crystallization of the D369N enzyme

The D369N enzyme was crystallized by vapor diffusion using hanging drops of 15 μL. The enzyme solution, at approximately 30 mg/mL, was first dialyzed against a 20% saturating solution of $(NH_4)_2SO_4$, 100 mM Tris, 10 mM $MgCl_2$, 0.01 mM $ZnCl_2$ at pH 9.5. Crystals formed in about 2 weeks in reservoirs where the ammonium sulfate was between 36 to 39% saturation. Before mounting in glass capillaries, the crystals were harvested and stabilized in a solution containing 65% saturating $(NH_4)_2SO_4$, 100 mM Tris, 10 mM $MgCl_2$, 10 mM $ZnCl_2$, and 2 mM NaH_2PO_4 at pH 7.5 (Kim & Wyckoff, 1991).

X-ray data collection

The diffraction data were collected at the Crystallographic Facility in the Chemistry Department of Boston College, using the San Diego Multiwire MARK III system, driven by a Micro VAX3500 computer linked to an RU-200 rotating-anode generator operated at 50 kV and 150 mA. One multiwire proportional counter (Cork et al., 1975; Xuong et al., 1985) was used and CuK_α radiation was obtained with a graphite monochromater. The detector was set at 106 cm from the crystal, and a helium pathway was placed between the detector and the crystal to minimize the effect of air scattering. The intensities of diffraction maxima were measured by using an ω scan at step intervals of 0.1°. The distance between the crystal and detector permitted measurement of diffraction maxima to 2.45 Å resolution. Of the 43,509 unique reflections possible to 2.5 Å, 42,809 were collected with an average redundancy of 7.5.

Merging of reflections

Merging of the diffraction data was accomplished by using the software provided by San Diego Multiwire (Howard et al., 1985). A scale factor was calculated for multiple measurements and symmetry-related reflections. Those measurements deviating substantially from the average for a particular reflection were manually deleted. This merging and editing procedure was repeated until outliers were no longer apparent. The final R_{sym}^2 was 8.5%.

$$2\ R_{sym} = \frac{\sum_{hkl} \sum_i |I_{mean} - I_i|}{\sum_{hkl} \sum_i I_i}.$$

Structural refinement

The initial model used to begin the refinement of the mutant enzyme structure was based on the coordinates of the wild-type *E. coli* alkaline phosphatase (kindly provided by Dr. Wyckoff) with the zinc, magnesium, phosphate, and solvent atoms removed. The aspartate side chain at position 369 was then replaced with asparagine using the sequence-editing features of QUANTA (Molecular Simulations, Inc.). Refinements were carried out using XPLOR versions 3.0 and 3.1 (Brünger, 1992), running on Silicon Graphics Indigo II workstations at Boston College and on the Cray Y-MP C90 at the Pittsburgh Supercomputer Center. The initial *R*-factor was 0.34. Lower *R*-factors and improved stereochemistry were obtained by positional refinement, temperature factor refinement, and simulated annealing. Scripts were written for running XPLOR noninteractively, based on the examples provided, using the parameter files param19x.pro and toph19x.pro. The parameter WA was set to 170,000. This value was approximately one-third the value determined by running the script check.inp on the unrefined structure. Interactive rebuilding of some side chains, using QUANTA, was required at several stages. Noncrystallographic symmetry restraints were introduced for the main-chain atoms, the side-chain atoms, and symmetry-related water molecules. At each stage of the refinement, additional water molecules were added at positions indicated by their density in omit maps. Temperature factors (B) of the solvent molecules were closely monitored during refinement. Coordinates of the water molecules with B values greater than 50 $Å^2$ were checked against the density at each round. These water molecules were deleted from the model or repositioned manually if they were outside the 0.8σ contour in $2F_o - F_c$ maps, where σ is the RMS deviation from the mean density. Coordinates from the final refinement have been deposited ited in the Brookhaven Protein Data Bank under entry code 1ALH.

References

Anderson RA, Bosron WF, Kennedy FS, Vallee BL. 1975. The role of magnesium in *Escherichia coli* alkaline phosphatase. *Proc Natl Acad Sci USA 72*:2989–2993.

Anderson RA, Kennedy FS, Vallee BL. 1976. The effect of Mg(II) on the spectral properties of Co(II) alkaline phosphatase. *Biochemistry 15*:3710–3715.

Bloch W, Bickar D. 1978. Phosphate binding to *Escherichia coli* alkaline phosphatase: Evidence for site homogeneity. *J Biol Chem 253*:6211–6217.

Bradford MM. 1976. A rapid and sensitive method for the quantitation of microgram quantities of protein utilizing the principle of protein-dye binding. *Anal Biochem 72*:248–254.

Brünger AT. 1992. *XPLOR, version 3.1.* New Haven, Connecticut: Yale University Press.

Chaidaroglou A, Brezinski JD, Middleton SA, Kantrowitz ER. 1988. Function of arginine in the active site of *Escherichia coli* alkaline phosphatase. *Biochemistry 27*:8338–8343.

Chen LC, Neidhart D, Kohlbrenner WM, Mandecki W, Bell S, Janusz, S, Abad-Zapatero C. 1992. Three-dimensional structure of a mutant

(Asp101 → Ser) of alkaline phosphatase with higher catalytic efficiency. *Protein Eng 5*:605-610.

Coleman JE. 1987. Multinuclear nuclear magnetic resonance approaches to the structure and mechanism of alkaline phosphatase. In: Torriani-Gorini A, Rothman FG, Silver S, Wright A, Yagil E, eds. *Phosphate metabolism and cellular regulation in microorganisms*. Washington D.C.: American Society for Microbiology. pp 127-138.

Coleman JE, Nakamura KI, Chlebowski JF. 1983. ^{65}Zn(II), ^{115}mCd(II), ^{60}Co(II), and Mg(II) Binding to alkaline phosphatase of *Escherichia coli*: Structure and functional effect. *J Biol Chem 258*:386-395.

Cork C, Hamlin R, Vernon W, Xuong NH. 1975. A xenon-filled multiwire area detector for X-ray diffraction. *Acta Crystallogr A 31*:702-703.

Dayan J, Wilson IB. 1964. The phosphorylation of tris by alkaline phosphatase. *Biochim Biophys Acta 81*:620-623.

Evans SV. 1993. SETOR: Hardware lighted three-dimensional solid model representations of macromolecules. *J Mol Graphics 11*:134-138.

Garen A, Leventhal C. 1960. A fine-structure genetic and chemical study of the enzyme alkaline phosphatase of *E. coli. Biochim Biophys Acta 38*:470-483.

Gettins P, Coleman JE. 1983a. ^{113}Cd nuclear magnetic resonance of Cd(II) alkaline phosphatase. *J Biol Chem 258*:396-407.

Gettins P, Coleman JE. 1983b. ^{31}P Nuclear magnetic resonance of phosphoenzyme intermediates of alkaline phosphatase. *J Biol Chem 258*:408-416.

Gettins P, Coleman JE. 1984a. Chloride binding to alkaline phosphatase. *J Biol Chem 259*:11036-11040.

Gettins P, Coleman JE. 1984b. Zn(II)-^{113}Cd(II) and Zn(II)-Mg(II) hybrids of alkaline phosphatase. *J Biol Chem 259*:4991-4997.

Gettins P, Metzler M, Coleman JE. 1985. Alkaline phosphatase. Probes of the mechanism. *J Biol Chem 260*:2875-2833.

Hough E, Hansen LK, Birknes B, Jynge K, Hansen S, Hordvik A, Little C, Dodson EJ, Derewenda Z. 1989. High-resolution (1.5 Å) crystal structure of phospholipase C from *Bacillus cereus. Nature (Lond) 338*:357-360.

Howard AJ, Nielsen C, Xuong NH. 1985. Software for a diffractometer with multiwire area detector. In: Timasheff SN, ed. *Methods in enzymology*. London: Academic Press. pp 452-471.

Hull WE, Halford SE, Gutfreund H, Sykes BD. 1976. ^{31}P nuclear magnetic resonance study of alkaline phosphatase: The role of inorganic phosphate in limiting the enzyme turnover rate at alkaline pH. *Biochemistry 15*:1547-1561.

Janeway CML, Xu X, Murphy JE, Chaidaroglou A, Kantrowitz ER. 1993. Magnesium in the active site of *Escherichia coli* alkaline phosphatase is important for both structure stabilization and catalysis. *Biochemistry 32*:1601-1609.

Jones SR, Kindman LA, Knowles JR. 1978. Stereochemistry of phosphoryl group transfer using a chiral [^{16}O, ^{17}O, ^{18}O] stereochemical course of alkaline phosphatase. *Nature (Lond) 275*:564-565.

Kim EE, Wyckoff HW. 1989. Structure of alkaline phosphatase. *Clin Chim Acta 186*:175-188.

Kim EE, Wyckoff HW. 1991. Reaction mechanism of alkaline phosphatase based on crystal structures. *J Mol Biol 218*:449-464.

Kunkel TA. 1985. Rapid and efficient site-specific mutagenesis without phenotypic selection. *Proc Natl Acad Sci USA 82*:488-492.

Kunkel TA, Roberts JD, Zakour RA. 1987. Rapid and efficient site-specific mutagenesis without phenotype selection. *Methods Enzymol 154*:367-382.

Laemmli UK. 1970. Cleavage of structural proteins during the assembly of the head of bacteriophage T4. *Nature (Lond) 227*:680-685.

Laskowski RA, MacArthur MW, Moss DS, Thornton JM. 1993. PROCHECK: A program to check the stereochemical quality of protein structures. *Acta Crystallogr 26*:283-291.

Lee B, Richards FM. 1971. The interpretation of protein structures: Estimation of static accessibility. *J Mol Biol 55*:379-400.

Luzatti PV. 1952. Traitement statistique des erreurs dans la determination des structures cristallines. *Acta Crystallogr 5*:802-810.

Murphy JE, Kantrowitz ER. 1994. Why are mammalian alkaline phosphatases much more active than bacterial alkaline phosphatases? *Mol Microbiol 12*:351-357.

Murphy JE, Xu X, Kantrowitz ER. 1993. Conversion of a magnesium binding site into a zinc binding site by a single amino acid substitution in *E. coli* alkaline phosphatase. *J Biol Chem 268*:21497-21500.

Plocke DJ, Vallee BL. 1962. Interaction of alkaline phosphatase of *E. coli* with metal ions and chelating agents. *Biochemistry 1*:1039-1043.

Schultz C, Bertini I, Viezzoli MS, Brown RD, Koenig SH, Coleman JE. 1989. Manganese(II) as a probe of the active center of alkaline phosphatase. *Inorg Chem 28*:1490-1496.

Schwartz JH, Lipmann F. 1961. Phosphate incorporation into alkaline phosphatase of *E. coli. Proc Natl Acad Sci USA 47*:1996-2005.

Sowadski JM, Foster BA, Harold WW. 1981. Structure of alkaline phosphatase with zinc/magnesium cobalt or cadmium in the functional metal sites. *J Mol Biol 150*:245-272.

Sowadski JM, Handschumacher MD, Murthy HMK, Foster BA, Wyckoff HW. 1985. Refined structure of alkaline phosphatase from *E. coli* at 2.8 Å resolution. *J Mol Biol 186*:417-433.

Sowadski JM, Handschumacher MD, Murthy HMK, Kundrot C, Wyckoff HW. 1983. Crystallographic observations of the metal ion triple in the active site region of alkaline phosphatase. *J Mol Biol 170*:575-581.

Trentham DR, Gutfreund H. 1968. The kinetics of the reaction of nitrophenyl phosphate with alkaline phosphatase from *Escherichia coli. Biochem J 106*:455-460.

Volbeda A, Lahm A, Sakiyama F, Suck D. 1991. Crystal structure of *Penicillium citrinum* P1 nuclease at 2.8 Å resolution. *EMBO J 10*:1607-1618.

Wilson IB, Dayan J, Cyr K. 1964. Some properties of alkaline phosphatase. *J Biol Chem 239*:4182-4185.

Xu X, Kantrowitz ER. 1991. A water-mediated salt link in the catalytic site of *Escherichia coli* alkaline phosphatase may influence activity. *Biochemistry 30*:7789-7796.

Xu X, Kantrowitz ER. 1992. The importance of aspartate 327 for catalysis and zinc binding in *Escherichia coli* alkaline phosphatase. *J Biol Chem 267*:16244-16251.

Xu X, Kantrowitz ER. 1993. Binding of magnesium in a mutant *E. coli* alkaline phosphatase changes the rate-determining step in the reaction mechanism. *Biochemistry 32*:10683-10691.

Xuong NH, Nielsen C, Hamlin R, Anderson D. 1985. Strategy for data collection from protein crystals using a multiwire counter area detector diffractometer. *J Appl Crystallogr 18*:342-350.